Analytical and Bioanalytical Chemistry (2021) 413:1715–1727
https://doi.org/10.1007/s00216-020-03140-3

RESEARCH PAPER

A colorimetric paper-based ATONP-ALP nanobiosensor for selective detection of Cd^{2+} ions in clams and mussels

Krishna Kumari Swain [1] · Sunil Bhand [1]

Received: 10 October 2020 / Revised: 6 December 2020 / Accepted: 21 December 2020 / Published online: 10 February 2021
© Springer-Verlag GmbH Germany, part of Springer Nature 2021

Abstract

A colorimetric paper-based enzyme-coupled antimony tin oxide nanoparticle (ATONP) nanobiosensor for selective detection of Cd^{2+} ions in clams and mussels is presented. Alkaline phosphatase (ALP) was immobilized on ATONPs via 16-phosphonohexadecanoic acid (16-PHA) to develop ATONP-ALP nanobiosensor. The biosensor was characterized using XPS, Raman spectroscopy, SEM, and EDX. ATONP-ALP nanobiosensor exhibited high selectivity towards detection of Cd^{2+} ion with a LOD 0.006 μg L^{-1} and linear range of detection 0.005–1 μg L^{-1}. The developed biosensor was further integrated into a low-cost paper-based format. A visual color change was obtained for Cd^{2+} ion in the range 0.1–10 μg L^{-1}. The developed biosensor was successfully demonstrated for the analysis of Cd^{2+} ions in clams with recoveries 101–104%. The ATONP-ALP nanobiosensor was validated using mussel tissue (BCR-668) and the conventional ICP-OES and ICP-MS techniques.

Keywords Paper-based sensor · Colorimetric method · Antimony tin oxide · Alkaline phosphatase · Cd^{2+} ion · Clams · Mussels

Introduction

Cadmium (II) (Cd^{2+}) is a non-essential and highly toxic metal, widely present in the biosphere [1, 2]. Huge application of fertilizers, fossil fuels, metal smelting, and waste incineration are the primary sources of discharge of Cd^{2+} into the environment [3, 4]. Upon entering the aquatic system, Cd^{2+} ions may enter the food chain via bottom sediments and get absorbed and accumulated into the aquatic bodies like clams and mussels, which further gets transferred into the human body through seafood consumption [5]. Prolonged exposure to Cd^{2+} ion may severely damage the liver, kidneys, lungs, and cardiovascular system [6, 7]. It has also been reported that Cd^{2+} ions act as a carcinogen-causing cellular and metabolic disorders in the human body [8]. Clams and mussels contain cysteine-rich proteins (metallothionein), having a sulfhydryl group [9]. These sulfhydryl groups of metallothionein bind to the Cd^{2+} ions and help in the accumulation of Cd^{2+} ions in different organs of clams and mussels, causing inhibition of their protein functions [10]. The World Health Organization (WHO) has set a permissible limit of 2 mg kg^{-1} Cd^{2+} ion in mollusks [11]. Food Safety and Standards Authority of India (FSSAI) has determined a tolerable limit of 2 mg kg^{-1} Cd^{2+} ion in mollusks [12]. Although the level of Cd^{2+} ion in clams and mussels is much lower, nowadays, consumers buy mollusks from the market with no information about their contamination level. Hence, it is the need of the hour to evaluate Cd^{2+} ion accumulation in clams and mussels to prevent its consumption by human beings.

Several conventional techniques have been reported for the analysis of Cd^{2+} ions, such as atomic absorption spectroscopy (AAS), inductively coupled plasma mass spectroscopy (ICP-MS), and inductively coupled plasma optical emission spectroscopy (ICP-OES). These methods are highly sensitive and selective; however, they require extensive sample preparation and need trained manpower [13–15]. Hence, there is a need for the development of a simple yet sensitive analytical method for the detection of Cd^{2+} ions in clams and mussels.

Recently, paper-based colorimetric sensors are gaining significant attention for the analysis of environmental contaminants [16]. Because of their simple fabrication procedure, easy to use and portable nature, they provide a simple and low-cost method for the determination of heavy metal ions [17]. They are generally made up of porous cellulose papers, which provide a substantial surface-to-volume ratio for analysis of target analyte [18]. As a novel bioanalytical tool, paper-based

✉ Sunil Bhand
sunilbhand@goa.bits-pilani.ac.in

[1] Biosensor Lab, Department of Chemistry, BITS Pilani K.K. Birla Goa Campus, Mormugao, Goa 403726, India

sensors can be integrated into several detection strategies such as optical and electrochemical techniques [19–22]. Colorimetric biosensors have recently been reported for rapid screening of Cd^{2+} ion contamination [23]. Among the reported colorimetric method, enzyme-based biosensors have gained attention due to their metal-binding property, simplicity, low cost, and stability [24, 25]. Metal-binding enzymes such as alkaline phosphatase (ALP) have been reported for the construction of sensitive biosensors [26]. ALP is a glycoprotein, which contains Zn^{2+} and Mg^{2+} ion in its active site. ALP catalyzes *para*-nitrophenyl phosphate (*p*-NPP) to form *para*-nitrophenol, which produces a yellow color.

The survey of the literature reveals that enzyme-decorated nanoparticle (NP)-based biosensors have emerged as novel nanobiosensors with improved sensitivity and stability [27, 28]. Antimony-doped tin oxide nanoparticles (ATONPs) have emerged as a novel biosensing probe [29–31]. The conductive nature, optical transparency, and high surface area of ATONPs make them ideal materials for biosensor development. The presence of Sb in ATONPs enhances the catalytic properties and stability of ATONPs in aqueous solutions. Functionalization of NPs through self-assembly monolayers (SAMs) provides a substantial binding site to crosslink the enzyme on the NP surface [32]. In this work, surface functionalization of ATONPs was achieved using 16-phosphonohexadecanoic acid (16-PHA) followed by the coupling of ALP enzyme. Herein, we report for the first time development of a colorimetric paper-based ATONP-ALP nanobiosensor for selective detection of Cd^{2+} ion and its application to clams and mussels. The biosensor was constructed by immobilizing ALP on ATONPs using 16-PHA as a crosslinker. The fabrication of the developed nanobiosensor was optimized and extensively characterized. The activities of developed biosensors were optimized and the K_m, V_{max}, LOD, and K_i were determined using a multi-plate reader in the photometric mode in 96-well plates. The selectivity of the ATONP-ALP nanobiosensor towards Cd^{2+} ion was achieved by the masking technique. ATONP-ALP nanobiosensor was integrated into a low-cost paper-based format and visible color change was observed. In order to translate the applicability of the biosensor in the real samples, three different digestion methods were evaluated for leaching of Cd^{2+} ions accumulated in clam and mussel. The best-suited method LyM_1 (lyophilization method) was used for further analysis. The developed method was cross-validated against certified reference mussel tissue (BCR-668) and ICP-OES and ICP-MS techniques using spiked samples. The results obtained using the ATONP-ALP nanobiosensor exhibited a good agreement with the conventional techniques and can be extended for practical use.

Experimental section

Materials and instrumentations

The chemicals used for the experiment were mostly analytical and guaranteed reagent (AR/GR). Antimony tin oxide nanoparticles (ATONPs) (average size < 50 nm, ≥ 99.5% trace metals) was purchased from Sigma-Aldrich, USA. Alkaline phosphatase enzyme (activity 1000 units (20 I.U. μL^{-1}), protein concentration 19.10 mg mL^{-1}, and specific activity 2 unit μg^{-1} protein) from calf intestine was purchased from Roche Diagnostics (Germany). CRM standard mussel tissue (BCR-668), certified cadmium ICP standard (1000 mg $L^{-1} \pm$ 2 mg L^{-1}), and Whatman nylon membrane filter papers (pore size 0.45 μm, diameter 47 mm) were purchased from Sigma-Aldrich. Whatman Grade 41 qualitative filter papers (pore size 25 μm) were purchased from Whatman, India. Methanol (99% pure), ethanol (99%), and N-hydroxysuccinimide (NHS) were all purchased from Merck (Germany). *p*-Nitrophenyl phosphate (*p*-NPP) and 16-phosphonohexadecanoicacid (16-PHA) were purchased from Sigma-Aldrich. N-(3-Dimethyl aminopropyl)-N′-ethyl carbodiimide hydrochloride (EDC) was purchased from Sigma (USA). O-Phenylenediamine dihydrochloride (OPD), sodium hydroxide (NaOH), trisodium citrate, and citric acid were obtained from Acros Organics (USA). Tris hydrochloride (tris buffer) and acetone were procured from Fisher scientific chemical (USA). Osmium tetroxide (OsO_4) was purchased from Sigma (USA). Mercury and lead AAS/ICP standard for environmental analysis were bought from Fluka analytical (Germany). Chromium, zinc, nickel, cobalt, and copper standards were obtained from Acros Organics (USA). Sodium dodecyl sulfate (SDS) was purchased from HIMEDIA (India). Disodium salt of ethylenediaminetetraacetic acid (EDTA) was purchased from Merck (India). Deionized water (D.I. water) was used from Arium 61316 water purification system, Sartorius (Germany).

VictorX4 2030 multi-plate reader Perkin Elmer (USA) was used for the measurement of enzymatic activity in photometric mode. The X-ray photoelectron spectra (XPS) were collected using PHI 5000 Versa Prob II (FEI Inc.). Raman spectrometer (LABRAM HR Horiba, France) was used to collect the Raman spectra at 532 nm wavelength. The surface micrograph of the sample was obtained using a scanning electron microscope (SEM) from Quantum FEG-250, MAC FEI (Netherlands). The coating was carried out by using sputter coater LEICAEM SE-200, MAC LEICA (USA), and elemental analysis was done by energy dispersive analysis of X-rays (EDX) from AMETEK (USA). Metal analysis in an environmental sample was done using high-resolution ICP-MS (Thermo Fisher Scientific, Germany at IIT Bombay India) and ICP-OES (Perkin Elmer, Model: Avio 200 at SICART Gujrat India). Micropipettes were from Eppendorf (Germany). Toshcon ultrasonic cleaner (Toshniwal Process Instruments

Pvt. Ltd. (India)) was used for sonication. Spinix shaker from Tarsons (India) was purchased for shaking purposes. White transparent bottom polystyrene 96-microwell plate was procured from Merck (India). pH meter from Eutech (Singapore) was used for adjusting pH. Clam and mussel samples were obtained from the local supermarket of Goa, India. All the results were recorded, analyzed, and plotted using OriginPro 8.0 software (Origin Lab Corporation, USA) and ChemDraw software.

Preparation of standard solutions

All the metal ion solution preparation and dilutions were made as per the safety guidelines. A stock solution of 50 mM Tris buffer was prepared by mixing Tris chloride (788 mg) in 100 mL of freshly obtained D.I. water. A series of dilutions of (5–50 mM) was prepared from the stock solution of Tris buffer. Optimization of the pH was carried out by varying the pH of the buffer solution from 5–11 pH. 0.1 M HCl and 0.1 N NaOH were used for pH adjustment. The stock solution of the ALP enzyme (0.2 I.U. μL^{-1}) was prepared in 100 μL of the Tris buffer solution. It was diluted up to 0.002 I.U. μL^{-1}. A stock solution of 100 mM *p*-NPP was prepared and a set of dilution (0.5–100 mM) was prepared for kinetic measurement. The stock solution of 100 μg L^{-1} Cd^{2+} ion was prepared from the original ICP standard Cd^{2+} ion solution (1000 mg $L^{-1} \pm 2$ mg L^{-1}). A series of dilutions of (0.005–10 μg L^{-1}) Cd^{2+} ion was prepared by adding the Millipore water into the stock solution. The pH of the dilutions was kept neutral. Individual standard solutions of Hg^{2+}, Cd^{2+}, Ni^{2+}, Pb^{2+}, Zn^{2+}, Cu^{2+}, Co^{2+}, and Cr^{3+} were prepared. All the solutions used for the analysis purpose were kept in the refrigerator for future work.

Design and fabrication of ATONP-ALP nanobiosensor

The construction and fabrication of ATONP-ALP nanobiosensor were based on the efficient immobilization of enzyme through SAMs (16-PHA) on the ATONP surface. The fabrication of ATONPs required two steps: (a) surface functionalization of ATONPs by SAMs and (b) ALP enzyme immobilization on SAM-functionalized ATONPs.

Surface functionalization of ATONPs by SAMs

Approximately 10 mg ATONPs was taken in a 2-mL Eppendorf tube and dispersed in a 0.5 mM ethanolic solution of 16-PHA. The reaction mixture was incubated and stirred for 48 h in a dancing shaker at RT (room temperature) followed by exhaustive rinsing with D.I. water to remove unbound carboxylic acid from ATONPs. Post-phosphonation, 16-PHA-modified ATONPs were activated with an equimolar mixture of 100 mM EDC/NHS for 3 h at RT. Post-incubation, the excess NHS ester monolayers were washed several times with D.I. water and were stored for further surface modification.

ALP immobilization on SAM-modified ATONPs

The immobilization of the ALP was performed by adding ALP (0.008 I.U μL^{-1}) onto the surface of SAM-modified ATONPs. The ALP-treated SAM-modified ATONPs were subjected to react under the covalent coupling mechanism for 36 h at 4 °C to form ATONP-ALP nanobiosensor. Then, the biosensor was rinsed with D.I. water and stored at 4 °C for further experimental analysis.

Construction of paper-based sensor

The paper-based sensor was designed using three layers of Whatman filter papers. The upper and lower layers were made of Whatman nylon membrane filter papers (pore size 0.45 μm, diameter 47 mm) to prevent the spreading of the solution. The middle layer was made of Whatman Grade 41 qualitative filter papers (pore size 25 μm). The paper-based sensor contained six circular micro thimbles. The diameter of each micro thimbles was 0.8 cm. The schematic diagram of the paper-based ATONP-ALP nanobiosensor was shown in Scheme 1.

Development of sample pre-treatment method

Dead clam (*Meretrix meretrix*) and mussel (*Perna viridis*), locally called "Tisri and Xinanneo," were obtained from the local supermarkets of the coastal area of Goa (India) during the period of July to November 2019. The samples were immediately stored in an ice-box and brought to the lab for further analysis. All the samples were washed in D.I. water and kept at RT. The cleaned samples were divided into two parts: (i) blank (non-spiked) samples and (ii) samples spiked with metal. Nowadays, the acid digestion method is commonly used for the pre-treatment of real samples. But the major drawback of this method is the use of a high amount of concentrated acids, which produces toxic gases and has high blank values. Hence, in order to optimize sample pre-treatment protocol, three different methods of sample digestion were selected, namely method 1: Lyophilization method (LyM_1); method 2: Homogenization method (HM_2); and method 3: Acid digestion method (AdM_3). Digestions were performed into a closed vessel. The detailed sample pre-treatment methods deployed for digestion of clam and mussel

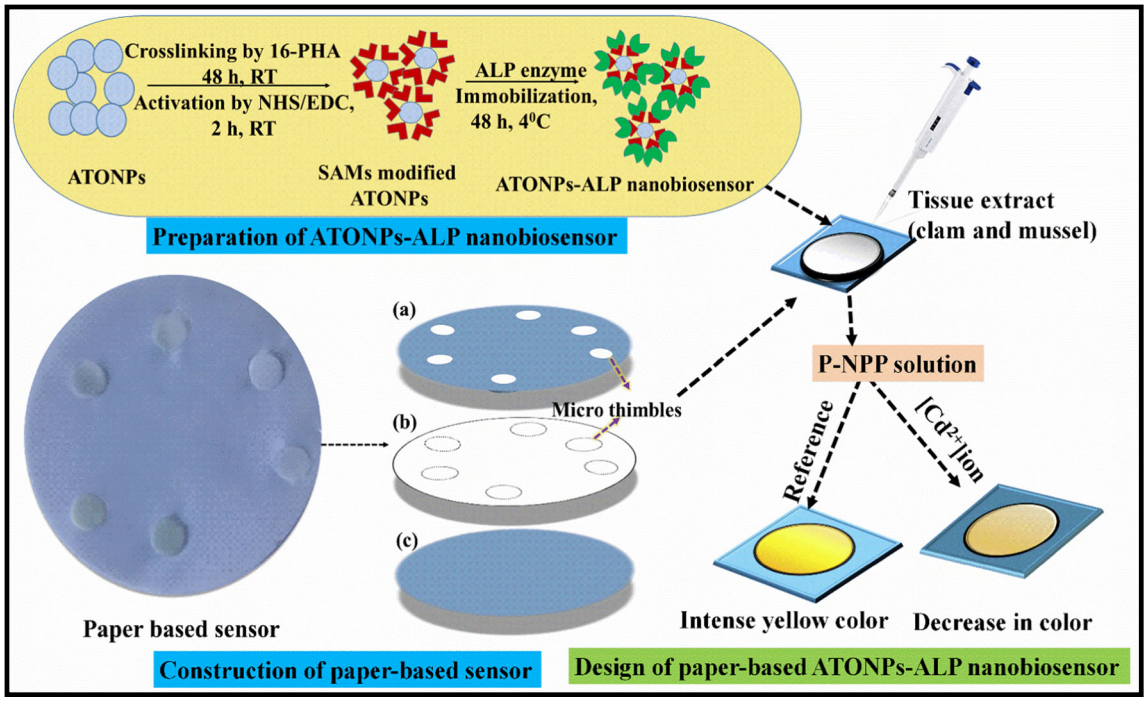

Scheme 1 Pictorial representation of a miniaturized, ATONP-ALP nanobiosensor integration to the paper-based format for the colorimetric detection of Cd^{2+} ion (**a**) upper layer made of nylon membrane filter paper, (**b**) middle layer made of Whatman filter paper, and (**c**) lower layer made of nylon membrane filter paper.

samples were mentioned in the Supplementary Information (ESM), supplementary text S1 and Table S2.

Biosensor principle and measurements

The principle and measurement of enzyme biosensor (ATONP-ALP nanobiosensor) were based on the inhibition of the enzyme by Cd^{2+} ions. Analytical performance of ATONP-ALP nanobiosensor was investigated by constructing a standard calibration curve under optimized conditions. This interaction of metal ions with enzyme forms a metal chelate complex in the active site of the enzyme, which results in blocking the path of enzyme-substrate interaction. As a result, the original enzyme-substrate activity was decreased with the addition of metal ions. The reduced enzyme activity was measured in terms of inhibition % by observing color changes at 405 nm, as mentioned in Eq. (1).

$$I\% = \left[\frac{I_0 - I_1}{I_0}\right] \times 100 \quad (1)$$

where

$I\%$ Degree of inhibition
I_0 Intensity of reference (without spiking of Cd^{2+} ions)
I_1 Intensity of Cd^{2+} ion-spiked sample

Results and discussions

Analytical parameters of nanobiosensor

The optimization of influential parameters, such as ionic strength, pH, enzyme concentration, and temperature profile, which can affect the activity of ATONP-ALP nanobiosensor was studied and presented as ESM, Fig. S1. All the experimental assays were accomplished with the working buffer (Tris buffer). The maximum activity was achieved at 25 mM for ATONP-ALP nanobiosensor (ESM, Fig. S1a). This was due to the improvement of the apparent affinity and binding capacity of ALP. As the ionic strength of buffer increases, the number of interaction sites present on the surface of ALP enzyme increases, which results in tight adsorption on the binding site. The optimization of pH of Tris buffer was carried out in the pH range 5–11. A maximum saturated signal intensity was observed at pH 9 (ESM, Fig. S1b). In the enzymatic assay, the concentration of enzyme plays an important role. The optimization of enzyme concentration was carried out by varying ALP concentrations in the range of 0.002–0.02 I.U. μL^{-1}. An optimal maximum intensity was obtained at 0.008 I.U. μL^{-1} of ALP enzyme and became saturated (ESM, Fig.

S1c). The rate of the enzyme-substrate reaction is proportional to the substrate concentration bound to the active site of the enzyme that leads to maximum response for the particular concentration. Hence, optimum enzyme concentration was achieved. The temperature profile of biosensor was studied in the range 25–45 °C (ESM, Fig. S1d). Since a reasonably good activity was observable at 25 °C (RT), further additional tests were performed at 25 °C.

Determination of kinetic parameters

The enzyme kinetic study of ATONP-ALP nanobiosensor was investigated using different substrate concentrations. The kinetics behavior was quantitatively expressed by Michaelis-Menten constant (K_m) and maximum velocity (V_{max}). K_m indicates how efficiently an enzyme immobilization and how much substrate is required in an enzymatic reaction to form its end product. The K_m value for the ATONP-ALP nanobiosensor was calculated using the Lineweaver-Burk plot, as presented in Eq. (2). To determine the K_m value, a varying range of *p*-NPP concentration (0.1–10 mM) was used (Fig. 1).

$$\frac{1}{V} = \frac{K_m}{V_{max}\,[S]} + \frac{1}{V_{max}} \tag{2}$$

where

V	Initial velocity
V_{max}	Maximum velocity
K_m	Michaelis-Menten constant
[S]	Substrate concentration (*p*-NPP) for enzymatic reaction

The response (absorbance) was recorded against the *p*-NPP concentration (0.1–10 mM) up to 10 min, as shown in Fig. 1a. The figures of merit of ATONP-ALP nanobiosensor (K_m, V_{max}, and regression coefficient R^2) were found to be 0.22 mM, 1.628, and 0.969, respectively (Fig. 1b). A lower value of K_m obtained for ATONP-ALP nanobiosensor signifies the higher affinity of the enzyme probe towards the substrate. This suggests the strong covalent immobilization of ALP enzyme on SAM-modified ATONPs.

Characterization of enzyme nanobiosensor

X-ray photoelectron spectroscopy and Raman spectroscopy

In order to determine the elemental composition and confirm the binding of crosslinker and enzymes to the ATONPs, the surface of the ATONP-ALP nanobiosensor was characterized by X-ray photoelectron spectroscopy (XPS) analysis. In the bare ATONPs, the elemental peak of Sn, Sb, and O were visible in the XPS spectrum (Fig. 2a). The peak at 495.6 eV and 485.5 eV corresponds to two transition states of Sn, i.e., $Sn3d_{3/2}$ and $Sn3d_{5/2}$, respectively. The consecutive peaks at 532 eV and 540 eV were attributed to the oxidation state of Sb, i.e., $Sb3d_{5/2}$ and $Sb3d_{3/2}$ transition state. From the abovementioned binding energy value, it was confirmed that Sb and Sn exhibited two oxidation states Sb^{3+}/Sb^{5+} and Sn^{3+}/Sn^{5+} in bare ATONPs [33]. The overlapping of the binding energy value of O and Sb at 530 eV represents both O1s and $Sb3d_{5/2}$ transition state, which further confirms that the O1s is directly bonded to a Sb atom (Sb-O). The peaks at 818 eV, 768 eV, 759.8 eV, and 718 eV corresponds to the $Sb3p_{1/2}$, $Sb3p_{3/2}$, $Sn3p_{1/2}$, and $Sn3p_{3/2}$, respectively. Figure 2c represents the XPS spectra of SAM-modified ATONPs. The peak at 138.7 eV represents P in the P2p region. Peaks at 285.1 and 399.84 eV corresponding to C1s and N1s suggest the successful surface functionalization of ATONPS by 16-PHA. XPS analysis was further carried out to confirm the binding of ALP to the surface of SAM ATONPs. Figure 2e corresponds to the XPS spectra of ATONP-ALP nanobiosensor. Binding energy (B.E) values 1036.55 eV and 1296.5 eV demonstrate the presence of Zn ($Zn2p_{3/2}$) and Mg (Mg1s), respectively, which are the two metal centers reported to be present in the

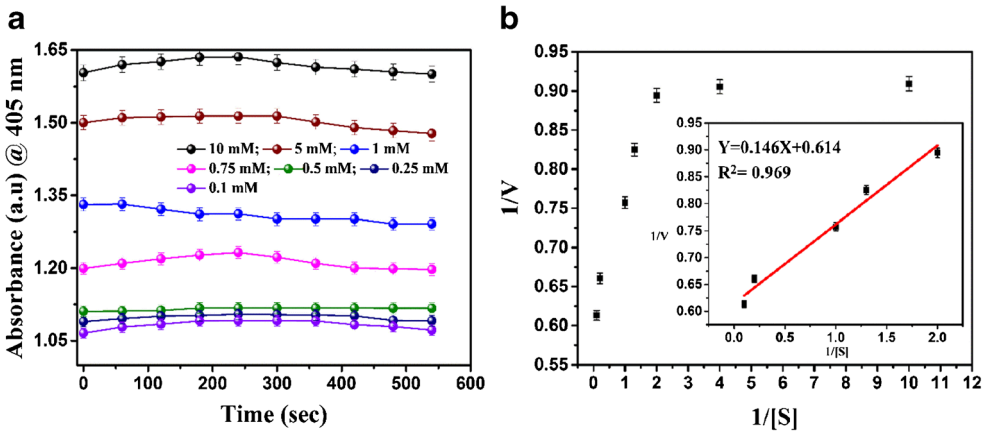

Fig. 1 **a** Response (absorbance) was recorded for the *p*-NPP concentration (0.1–10 mM) up to 10 min in 25 mM Tris buffer (pH 9.0) at 405 nm using a multiplate reader in the photometric mode. **b** Lineweaver-Burk plot obtained for the activity of ATONP-ALP nanobiosensor at 240 s (optimum response) under optimal conditions; *p*-NPP (0.1–10 mM) in 25 mM of Tris buffer pH 9.0 at 27 °C (inset: linear fit in logarithmic scale)

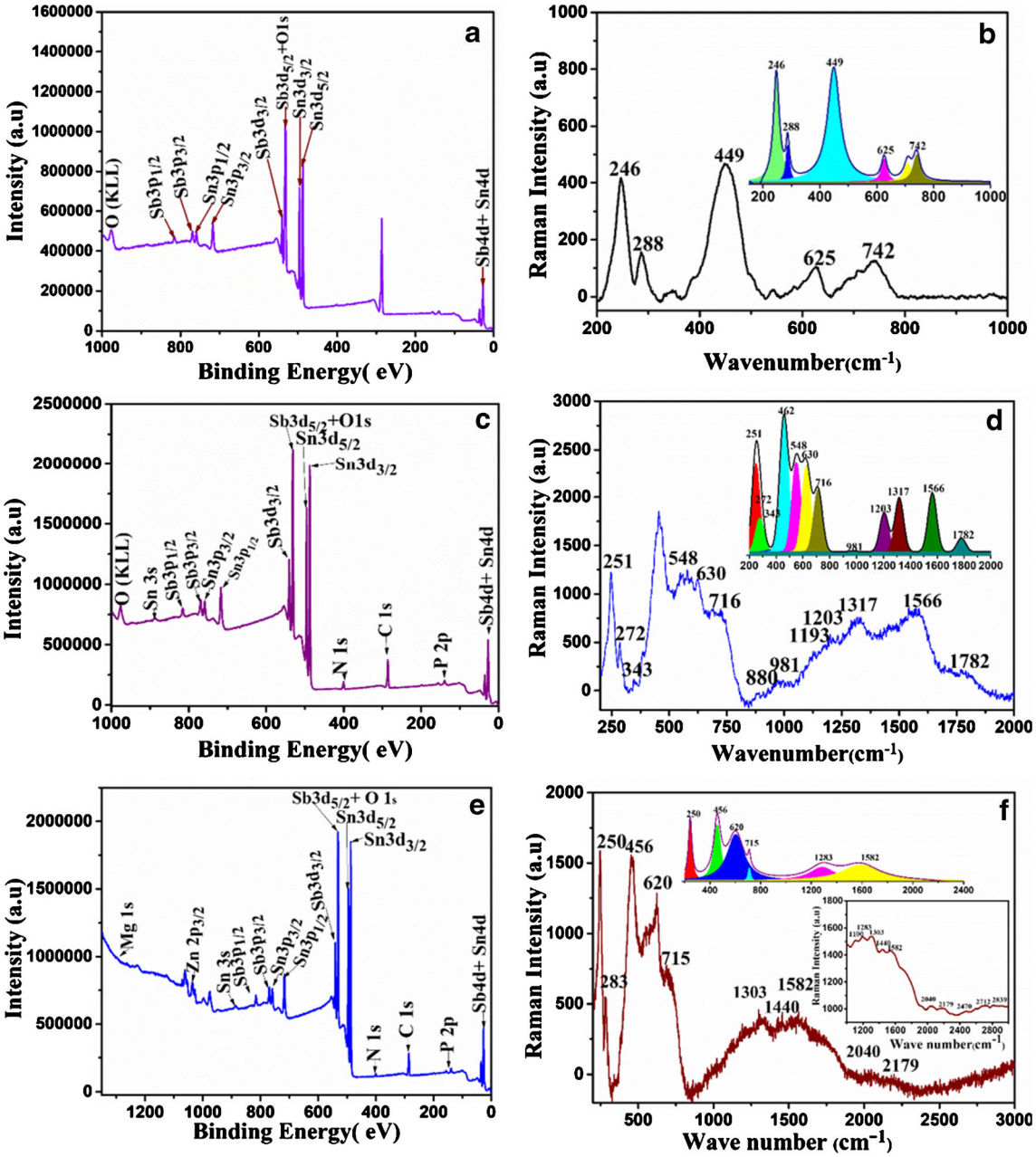

Fig. 2 **a** XPS spectra of bare ATONPs. **b** Room temperature Raman spectra of bare ATONPs (inset: Lorentz peak fitted plot assigned to main peaks from 200 to 1000 cm^{-1}). **c** XPS spectra of SAM-modified ATONPs. **d** Raman spectra of SAM-modified ATONPs (inset: Lorentz peak fitted plot assigned to main peaks from 200 to 2000 cm^{-1}). **e** XPS spectra of ATONP-ALP nanobiosensor and **f** Raman spectra of ATONP-ALP nanobiosensor (inset: main peaks from 1000 to 2900 cm^{-1} range were chosen for better clarity of spectra; Lorentz peak fitted plot assigned to main peaks from 200 to 2400 cm^{-1})

active site of ALP. These XPS measurements strongly signify the covalent binding between the ALP and the surface of ATONPs.

In order to explore the conformational and structural changes on the surface of ATONPs before and after immobilization of ALP, room temperature Raman spectroscopy analysis was carried out at 532 nm using Nd-YAG laser 100 mW with lateral resolution ~5 μm. Raman spectra of bare ATONPs were presented in Fig. 2b. The main peaks were fitted by a Lorentzian peak fit model shown inside the main figure. The spectral band at 246 and 288 cm^{-1} were attributed to Raman vibrational modes of SbO_2. The significant peaks at 449, 625, and 742 cm^{-1} correspond to three fundamental bands of SnO_2 sample [34]. Figure 2d represents the SAM-modified ATONPs. The bands at 548 and 981 cm^{-1} were assigned to the

asymmetric bending mode of PO_4. Peaks at 1193 and 1317 cm^{-1} correspond to the C–C stretching vibration and $–CH_2$ twist plane mode. The ester monolayer (–COOR) was confirmed from bands present at 1566 and 1782 cm^{-1}. The amide group (–CO–NR) was confirmed from the Raman vibrational mode at 1317 cm^{-1}. From the above peaks, it was confirmed that there was a successful crosslinking of SAMs on ATONPs. In order to investigate the surface modification after covalent immobilization of ALP on SAM-modified ATONPs, Raman analysis was performed for ATONP-ALP nanobiosensor (Fig. 2f). The fingerprint Raman spectra at 2040 cm^{-1} represent the C-H str. vibration of ATONP-ALP nanobiosensor. The C=C group of the developed biosensor was observed at 2179 cm^{-1}. The vibrational band at 2470 cm^{-1} confirms the presence of –SH group in ATONP-ALP nanobiosensor (the confirmation of –SH group may be due to the presence of cysteine in ALP) [35]. The Raman spectra at 2712 and 2839 cm^{-1} signify the primary and secondary C-H str. vibration mode of ATONP-ALP nanobiosensor. Hence, in conclusion, considering the above fingerprint peaks of ATONP-ALP nanobiosensor, it confirms the strong covalent bonding between ALP and SAM-modified ATONPs.

Scanning electron microscopy and energy dispersive X-ray analysis

Surface morphology and elemental analysis of bare, SAM-modified ATONPs and ATONP-ALP nanobiosensor were characterized using scanning electron microscope (SEM) and energy dispersive X-ray (EDX) technique. The SEM sample preparation methods were performed as per the reported literature (mentioned in the ESM, supplementary Text S2) [36]. From the SEM micrograph, it was observed that the bare ATONPs were spherical in size, with an average particle size of 28 ± 13.63 nm (ESM, Fig. S2a). The presence of the main elements such as Sb and Sn in bare ATONPs was confirmed from EDX analysis (ESM, Fig. S2b). The coagulation of ATONPs was observed as visualized from the SEM of SAM-modified ATONPs (ESM, Fig. S2c). The presence of C, O, N, and P from 16-PHA on ATONPs were confirmed from EDX spectra (ESM, Fig. S2d). The surface morphology of ATONP-ALP nanobiosensor with the main principal elemental peaks was spotted using SEM and EDX, as presented in ESM, Fig. S2e–f. From the micrograph, it was confirmed that after ALP immobilization on ATONPs, the surface exhibits a visibly rough and coagulated structure of NPs.

The SEM analysis of bare clam and mussel samples was performed and presented in ESM, Fig. S3a–b. From the EDX spectra (ESM, Fig. S3c–d) of bare clam and mussel samples, it was noted that the sulfur peak was obtained with 0.6 and 0.9 wt%, which strongly implies the presence of metallothionein in clam and mussel. In order to check the effect of Cd^{2+} ion on the surface of clam and mussel tissue, the tissue samples were soaked and incubated with 1 μg L^{-1} concentrations of cadmium ion solution. The EDX analysis was performed on cadmium-spiked clam and mussel tissue and represented as ESM, Fig. S3e–f. The EDX image (ESM, Fig. S3g–h) confirms the presence of a cadmium peak on the spiked surface samples.

Analytical performance of ATONP-ALP nanobiosensor

Calibration curve for ATONP-ALP nanobiosensor and paper-based ATONP-ALP nanobiosensor

In order to determine the analytical performance of the developed biosensor, inhibition measurements were carried to determine the reduction in ATONP-ALP nanobiosensor activity in the presence and absence of Cd^{2+} ion, using a colorimetric assay. All the measurements were carried out under an optimized condition of influential parameters in triplicate. The ATONP-ALP nanobiosensor assay consisted of Tris buffer (94 μL; 25 mM and pH 9.0), ATONP-ALP nanobiosensor (5 μL; 0.03 mg), and *p*-NPP solution (5 μL; 1 mM). For blank measurement, all the reaction ingredients were mixed up consecutively in a well of transparent 96-microwell plate. The reaction mixtures were incubated for a different period to allow the reactions to reach its equilibrium point. A maximum signal was observed for 15-min incubation time for ATONP-ALP nanobiosensor. After equilibrium, a pale yellow color was produced, which was further stopped by a stop solution of HCl (0.1 N; 50 μL) and measured using a multi-plate reader in photometric mode at 405 nm.

The calibration curve for Cd^{2+} analysis was obtained using ATONP-ALP nanobiosensor assay (Fig. 3a). A dynamic range of 0.005–10 μg L^{-1} concentration of Cd^{2+} ion ($[Cd^{2+}]$ ion) was studied to construct a standard calibration curve. A low limit of quantification (LOQ) 0.019 μg L^{-1} and a low limit of detection (LOD) 0.006 μg L^{-1} with a linear regression coefficient (R^2) of 0.947 was obtained. The order of sensitivity of ATONP-ALP nanobiosensor towards Cd^{2+} ions was 9% inhibition per decade. The maximal 50% inhibition (IC_{50}) was found to be 0.01 μg L^{-1}. The type of inhibition and inhibition constant (K_i) of ATONP-ALP nanobiosensor was obtained from the Dixon plot using different substrate and $[Cd^{2+}]$ ions (ESM, Fig. S4). From the Dixon plot, it was confirmed that only a minimal change in IC_{50} happens with a change in substrate concentration, suggesting a non-competitive inhibition mechanism as also reported in the literature [37]. K_i of the biosensor was found to be 0.088 nM, respectively. The smaller the value of K_i, the higher the binding affinity and the lower the amount of inhibitor required to inhibit the activity of the enzyme.

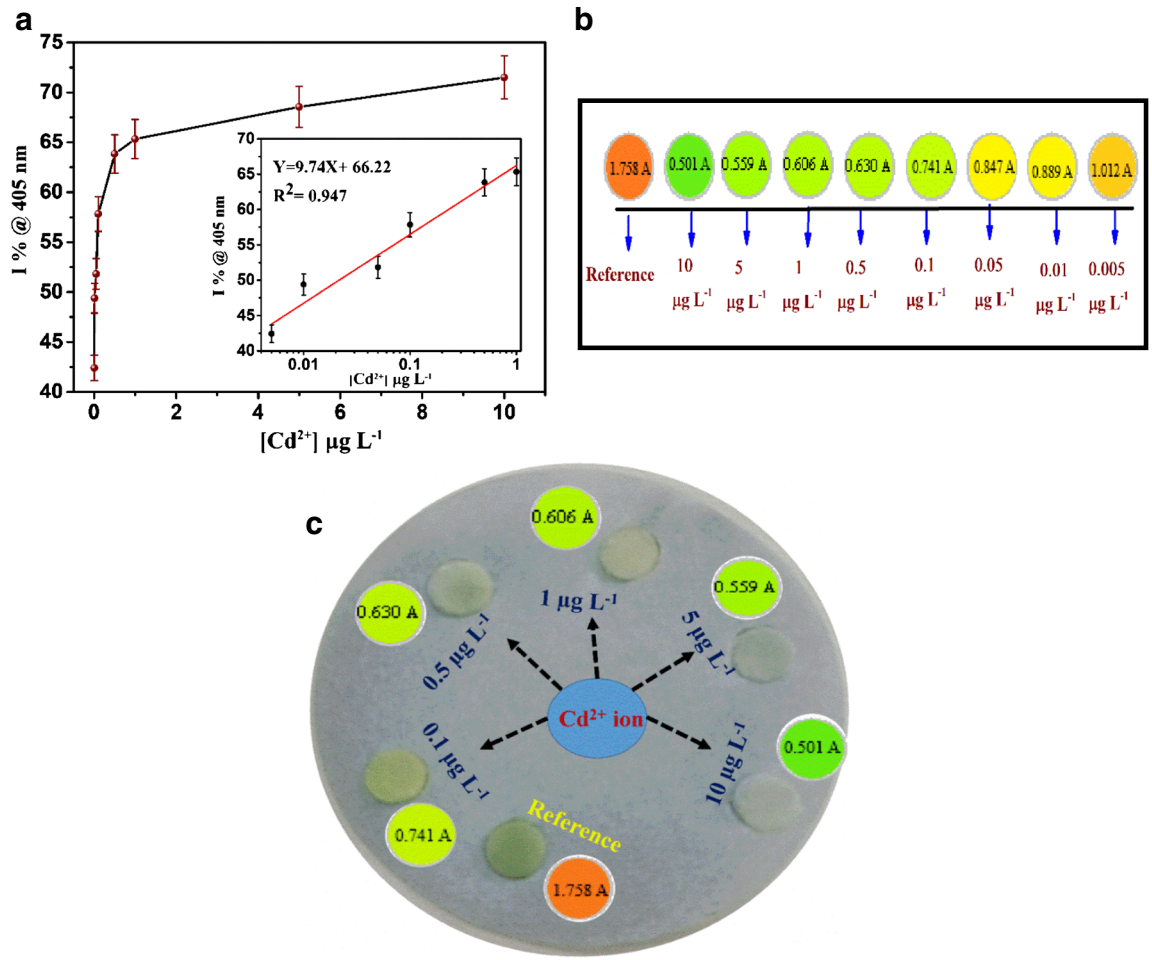

Fig. 3 **a** Calibration curve for Cd^{2+} ion inhibition obtained using ATONP-ALP nanobiosensor in the working range 0.005–10 µg L^{-1} (inset: linear calibration range 0.005–1 µg L^{-1}). The error bars represent the standard deviation of $n = 3$ (where n is the number of inhibition assays performed individually). **b** The color index of the individual concentration of Cd^{2+} with respect to reference was measured for ATONP-ALP nanobiosensor. **c** Illustration of visual detection of Cd^{2+} ion (0.1–10 µg L^{-1}) using paper-based ATONP-ALP nanobiosensor with the color index of the individual concentration of Cd^{2+} compared with the intensities measured at 405 nm using an Opti-plate reader

The values of K_m and K_i obtained for ATONP-ALP nanobiosensor exhibited a more significant interaction between substrate and inhibitor towards enzyme inhibition with higher % sensitivity per inhibition. The figures of merit of the developed Cd^{2+} ion inhibition assay under optimal conditions were presented in ESM, Table S2. The color corresponding to inhibition by varying concentration of Cd^{2+} over the reference (blank) was measured using ATONP-ALP nanobiosensor presented in Fig. 3b.

The analytical performance of paper-based ATONP-ALP nanobiosensor was studied by drop-casting ATONP-ALP nanobiosensor on the surface of a filter paper in the presence and absence of Cd^{2+} ion. Briefly, 10 µL of assay solution (buffer + ATONP-ALP nanobiosensor) was placed over six micro thimbles followed by the addition of 2 µL of [Cd^{2+}] ion solution (0.1–10 µg L^{-1}; 10-min incubation time) drop by drop into the five micro thimbles. One of the micro thimbles was kept as reference (without addition metal ion). Approximately 4 µL of *p*-NPP was added to all micro thimbles and incubated for 2 min. A sharp visible color change was noticed from the reference assay to the metal ion added assay. An intense yellow color was observed at the reference sample due to the formation of *p*-nitrophenol compound, whereas a decrease in intensity of yellow color was observed for samples with Cd^{2+} ion in the range 0.1–10 µg L^{-1}. The change in color of the developed assays was shown in Fig. 3c. The intensity of color corresponding to inhibition by varying concentration of Cd^{2+} ions over the reference (blank) was measured using an Opti-plate reader at 405 nm. From Fig. 3c, the disappearance of yellow color was indistinguishable for 5 and 10 µg L^{-1} of Cd^{2+} ions and the yellow color was visible up to 1 µg L^{-1}. Hence, the visual detection limit (LOD_{vis})

Table 1 Comparison of the detection limit of our developed method with other reported analytical methods for Cd^{2+} ion analysis

Receptor	Transducer	Linear range (μg L^{-1})	Detection limit (LOD μg L^{-1})	Reference
L-Cysteine Au-Ag NPs	Colorimetric	0.04–4323	4.92	[38]
Monoclonal antibody	Colorimetric	0.15–18	5	[39]
Aptasensor-PicoGreen	Fluorometric	100–1×10^5	0.038	[40]
Aptamer-AuNPs	Colorimetric	2–20	1.12	[41]
Pt/PANI-co-PDTDA/HRP	Amperometric	560–3800	96	[42]
ATONP-ALP nanobiosensor	Colorimetric	0.005–1	0.005	This work

for Cd^{2+} ion was found to be 1 μg L^{-1}. This implies that the developed paper-based colorimetric ATONP-ALP nanobiosensor can be deployed for the rapid screening of Cd^{2+} ions. The main advantages of paper-based colorimetric ATONP-ALP nanobiosensor were (a) the short analysis time, (b) miniaturized and easy to handle, and (c) low cost and easy to fabricate.

A comparison study of our developed method with other reported analytical methods for Cd^{2+} ion analysis is presented in Table 1.

Selectivity and interference studies

The selectivity of ATONP-ALP nanobiosensor and its effect on the presence of different mono, bi, and trivalent metal ions (Hg^{2+}, Cu^{2+}, Pb^{2+}, Zn^{2+}, Ni^{2+}, Na^{+}, K^{+}, Co^{2+}, Cd^{2+}, Cr^{3+}, Fe^{2+}, and Fe^{3+}) were investigated. Two fixed [Cd^{2+}] specifically 1 μg L^{-1} and 10 μg L^{-1} were taken for interference study to understand the influence on inhibition at lower and higher concentrations. To minimize the interference of coexisting ions, the effectiveness of the masking technique was investigated. Three types of masking agents were studied, namely citrate buffer for Cu^{2+} ion (3 μL, 0.025 M, and pH 5.0), acetate buffer (5 μL, 0.1 M, and pH 5.5) for Pb^{2+} and Zn^{2+} ions, and EDTA for Hg^{2+} ions (4 μL, 0. 25 M, and pH 5.0) [43, 44]. The experiment consists of a reaction mixture of Tris buffer (94 μL; 25 mM and pH 9.0), ATONP-ALP nanobiosensor (5 μL, 0.20 mg), individual metal ion solution (such as Ni^{2+}, Na^{+}, K^{+}, Co^{2+}, Cd^{2+}, Cr^{3+}, Fe^{2+}, and Fe^{3+} ions (2 μL, 1 μg L^{-1}, and 10 μg L^{-1})), and masked metal ion solution (Cu^{2+}, Zn^{2+}, Pb^{2+}, and Hg^{2+} ions). Then, 5 μL of *p*-NPP solution (1 mM) was added to the above reaction mixture and incubated for 10 min and measured at 405 nm in photometric mode. The inhibition of ATONP-ALP nanobiosensor in the presence of these metal ions with and without masking agents is presented in the ESM, Fig. S5. From the result, it was observed that in the presence of different individual metal ions, there was no significant influence on the inhibition of ATONP-ALP nanobiosensor by Cd^{2+} ions (ESM, Fig. S5a). Among the ten individual elements tested for the possible coexistence and interference, only four elements (namely Hg^{2+}, Pb^{2+}, Cu^{2+}, and Zn^{2+}) were found to be significantly higher than > 20%. However, in the construction curve using inhibition assay, the inhibition signal corresponding to analyte concentration more than 20% is considered. Hence, the possible interference was taken care of by masking their signals to 20% or lower in real sample analysis. Interfering metal ions such as Cu^{2+}, Pb^{2+}, and Zn^{2+} could be masked successfully as revealed by inhibition results (ESM, Fig. S5b). In the case of EDTA used as a masking agent, the inhibition results in the presence of Hg^{2+} and Cd^{2+} ion differ significantly. However, it cannot be practically deployed in masking of Hg^{2+} ion due to the fact that Cd^{2+}ion also gets co-precipitated alongside Hg^{2+} ion. This is due to its high affinity for EDTA (K_f = 16).

Reproducibility and stability

In order to ascertain the reproducibility of the developed method, various experiments were performed in batches (n = 10) and data were represented as ESM, Fig. S6. The results were found to be within 95% confidence limit and RSD values ± 4.3. To determine the stability of the ATONP-ALP nanobiosensor, the activity of the biosensor was tested over up to 30 days (ESM, Fig. S7). It can be observed that the activity of the biosensors exhibited good storage stability up to 30 days (retaining 73% of its original activity) when stored at 4 °C.

Analysis of the real sample

Standard addition method in real samples

The practicality of developed ATONP-ALP nanobiosensor in the clams and mussels was studied by using the standard addition method. In this experiment, different digestive samples from three different digestion methods were taken, matrix-matched, and then masked by adding masking agents to avoid the interference of other metal ions. Real samples were spiked with a known amount of [Cd^{2+}] ion (0.1 and 1 μg L^{-1}) and measured along with a blank sample (non-spiking). The [Cd^{2+}] ion added before and after spiking in real samples were calculated for three different digestion methods and compared

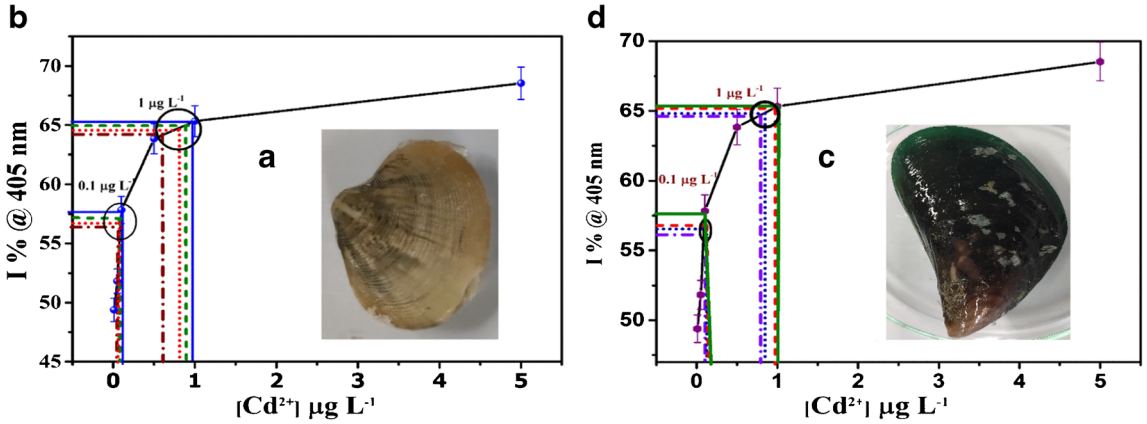

Fig. 4 Image of **a** clams (*Meretrix meretrix*). **b** Calibration curve obtained using standard addition method for Cd^{2+} ions in clams (•••) for standard curve, (--) LyM_1, (•••) HM_2, (-•-) AdM_3. **c** Mussels (*Perna viridis*). **d** Standard addition method of Cd^{2+} ions in mussels (-) for standard curve, (--) LyM_1, (•••) HM_2, (-.-) AdM_3 using three different digestion method under identical optimal conditions

with the standard calibration curve (Fig. 4). From the obtained data, it was found that three digestion methods, namely LyM_1, HM_2, and AdM_3 methods, show good recoveries in clams (102–104% for 1 µg L^{-1} and 101–103% for 0.1 µg L^{-1}) and mussels (100–102% for 1 µg L^{-1} and 101–103% for 0.1 µg L^{-1}). The average I % of ATONP-ALP nanobiosensor recorded using three different methods was found to be 64.57 ± 0.56% for 1 µg L^{-1} and 57.02 ± 0.48% for 0.1 µg L^{-1} in clams and 64.84 ± 0.20% for 1 µg L^{-1} and 56.76 ± 0.44% for 0.1 µg L^{-1} in mussels, which implies a good agreement with the standard calibration curve.

LyM_1 exhibited the highest inhibition % with good recoveries (100–101%) for both the clams and mussels among all the three tested methods; hence, it was selected as the best digestion method for further analysis. The detailed analysis of the standard addition method and comparison among three digestion methods for the real samples were given in Table 2.

Validation of the developed method

The accuracy and precision of the developed nanobiosensor for determination of Cd^{2+} in clam and mussel samples were validated against CRM standard mussel tissue BCR-668, ICP-OES, and ICP-MS technique. For ICP-OES analysis, blank and spiked samples were prepared by adding 1 µg L^{-1} of Cd^{2+} to the digested real sample. The samples were also measured simultaneously using the developed ATONP-ALP nanobiosensor. The results obtained from the ICP-OES analysis revealed that cadmium was not detectable in the blank sample, whereas 1.015 ± 0.04 µg L^{-1} and 1.009 ± 0.026 µg L^{-1} cadmium were found in spiked clams and mussels through the ICP-OES technique and 0.99 ± 0.003 µg L^{-1} [Cd^{2+}] in clams and 0.960 ± 0.012 µg L^{-1} [Cd^{2+}] in mussels were obtained using the developed ATONP-ALP nanobiosensor. In order to check the lower concentration of cadmium in real samples, the ICP-MS technique was utilized for validation (as ICP-OES was not sensitive enough at a lower concentration). Thus, a lower concentration of 0.1 µg L^{-1} Cd^{2+} was spiked with clam and mussel extracts. Both blank and spiked samples were analyzed and compared with the proposed biosensor technique. From the analysis, it was found that no cadmium was detected in the blank sample and a total cadmium concentrations of 0.109 ± 0.01 µg L^{-1} (for clams) and 0.111 ± 0.06 µg L^{-1} (for mussels) were detected in the spiked sample. Similarly, a lower concentrations of 0.097 ± 0.025 µg L^{-1} (for clams) and 0.099 ± 0.006 (for mussels) were obtained for spiked samples using the ATONP-ALP nanobiosensor assay.

Table 2 Metal ions found using different digestion methods (before and after spiking with real samples)

Sample	Cd^{2+} added (µg L^{-1})	Cd^{2+} found (µg L^{-1})		
		LyM_1	HM_2	AdM_3
Clam	0	0	0	0
	1	0.99±0.003	0.81±0.002	0.80±0.002
	0.1	0.097±0.025	0.082±0.001	0.079±0.015
Mussel	0	0	0	0
	1	0.96±0.003	0.84±0.002	0.78±0.002
	0.1	0.099±0.006	0.098±0.004	0.093±0.001

Table 3 Metal contents determined in spiked clams and mussels by ATONP-ALP nanobiosensor and cross-validated with mussel tissue BCR-668 and ICP-OES and ICP-MS technique

Sample	Cd^{2+}added ($\mu g\ L^{-1}$)	Cd^{2+} found ($\mu g\ L^{-1}$)			
		Proposed method (ATONP-ALP nanobiosensor)		ICP-OES*	ICP-MS*
		Real sample	Mussel tissue BCR-668		
Unspiked clams	0	Not detected	Not detected	Not detected	Not detected
Spiked clams	1	0.99±0.003	1.001±0.002	1.015±0.04	–
Spiked clams	0.1	0.097±0.025	0.099±0.003	–	0.109±0.01
Unspiked mussels	0	Not detected	Not detected	Not detected	Not detected
Spiked mussels	1	0.960±0.012	1.001±0.002	1.009±0.026	–
Spiked mussels	0.1	0.099±0.006	0.099±0.003	–	0.111±0.06

*Analyzed using external testing services

Additionally, the developed biosensor was tested and validated using mussel tissue BCR-668. The experiment was conducted on both the unspiked and spiked mussel tissue BCR-668. In the unspiked BCR-668, cadmium was not detected. While on the contrary, a total [Cd^{2+}] of $1.001 \pm 0.002\ \mu g\ L^{-1}$ (for $1\ \mu g\ L^{-1}$ [Cd^{2+}]) and $0.099 \pm 0.003\ \mu g\ L^{-1}$ (for $0.1\ \mu g\ L^{-1}$ [Cd^{2+}]) was obtained in the spiked BCR-668. The validation data of ATONP-ALP nanobiosensor by mussel tissue BCR-668 and ICP-OES/MS technique was shown in Table 3. From Table 3, it was observed that the BCR-668, ICP-OES, and ICP-MS data make a good match with the developed ATONP-ALP nanobiosensor data. Hence, it was strongly confirmed that the developed biosensor technique is much more efficient and holds practicability to determine the cadmium concentration in real environmental samples.

To investigate the presence of organic matter in the clams and mussels, total carbon analysis (TOC) was conducted to confirm the minimization of interference of organic carbon in real samples using the LyM_1 digestion protocol. The recovery % of different samples using ATONP-ALP nanobiosensor was calculated and were given in Table 4. From the table, the recovery % of the clams and mussels was estimated in a range of 101 to 104%.

Conclusion

Seafood (clam and mussels) contamination by Cd^{2+} ions is a serious threat to human health and the entire food chain system. There is an urgent need to develop a low cost and sensitive, rapid screening method for the rapid screening of [Cd^{2+} ions] in seafood and hence making awareness among consumers, to minimize human exposure to Cd^{2+} ion seafood. In summary, we demonstrate, for the first time, a paper-based colorimetric ATONP-ALP nanobiosensor for rapid

Table 4 Recoveries from real samples using LyM_1 digested method and analyzed by using ATONP-ALP nanobiosensor

Places	Matrix	Absorbance of Cd^{2+} (10 ng L^{-1})		Mean ± SD	RSD%	Recovery %	TOC ($\mu g\ L^{-1}$) Mean ±SD
		Before spiking	After spiking				
Zuarinagar	Clam sample 1	0.889	0.930	0.930 ± 0.037	3.971	104	1086 ± 78
	Clam sample 2	0.889	0.928	0.928 ± 0.005	0.538	104	1237 ± 51
	Mussel sample 1	0.889	0.897	0.897 ± 0.005	0.589	101	1046 ± 87
	Mussel sample 2	0.889	0.908	0.908 ± 0.012	1.325	102	1239 ± 32
Margao	Clam sample 1	0.889	0.929	0.929 ± 0.010	1.076	104	1024 ± 28
	Clam sample 2	0.889	0.908	0.908 ± 0.011	1.211	103	1466 ± 49
	Mussel sample 1	0.889	0.904	0.904 ± 0.006	0.719	102	1057 ± 58
	Mussel sample 2	0.889	0.913	0.913 ± 0.012	1.314	102	1069 ± 75
Panaji	Clam sample 1	0.889	0.915	0.915 ± 0.012	1.311	103	1055 ± 58
	Clam sample 2	0.889	0.921	0.921 ± 0.009	0.977	104	1037 ± 63
	Mussel sample 1	0.889	0.908	0.908 ± 0.005	0.550	102	1232 ± 23
	Mussel sample 2	0.889	0.915	0.915 ± 0.012	1.311	103	1060 ± 53

analysis of Cd^{2+} ions in clams and mussels. A significantly low limit of detection 0.006 μg L^{-1} with a linear working range 0.005–1 μg L^{-1} for Cd^{2+} ion was achieved. The sensitivity of ATONP-ALP nanobiosensor was found to be 9% per decade with an assay volume of 100 μL and 10-min analysis time. The selectivity of the biosensor towards Cd^{2+} ions was achieved by using masking agents. Good storage stability with 95% reproducibility was achieved. The ATONP-ALP nanobiosensor was integrated into a simple paper-based sensor to get an instant naked eye color change result. The developed ATONP-ALP nanobiosensor was successfully demonstrated for the analysis of Cd^{2+} ion-spiked seafood samples such as clam and mussel. An optimal sample pre-treatment protocol (LyM_1) was optimized to achieve good recoveries and reduce the consumption of hazardous chemicals. The validation of the ATONP-ALP nanobiosensor using CRM mussel tissue (BCR-668) and external laboratory validation provides a strong basis for the practical application of the developed method.

Supplementary Information The online version contains supplementary material available at https://doi.org/10.1007/s00216-020-03140-3.

Acknowledgments The authors acknowledge the CSIF Facility of BITS Goa and Hyderabad Campuses.

Funding Sunil Bhand acknowledges DAE-BRNS, India, for funding the project. Krishna Kumari Swain acknowledges BITS Pilani K.K. Birla Goa Campus for providing the fellowship.

Compliance with ethical standards

The research was conducted as per the Indian ethical guidelines for seafood.

Conflict of interest The authors declare that they have no conflict of interest.

References

1. Reimann C, Fabian K, Flem B. Cadmium enrichment in topsoil: separating diffuse contamination from biosphere-circulation signals. Sci Total Environ. 2019;651:1344–55.
2. Mezynska M, Brzóska MM. Environmental exposure to cadmium—a risk for health of the general population in industrialized countries and preventive strategies. Environ Sci Pollut Res. 2018;25(4):3211–32.
3. Nriagu JO, Pacyna JM. Quantitative assessment of worldwide contamination of air, water and soils by trace metals. Nature. 1988;333(6169):134–9.
4. Dharma-wardana MWC. Fertilizer usage and cadmium in soils, crops and food. Environ Geochem Health. 2018;40(6):2739–59.
5. Simpson W. A critical review of cadmium in the marine environment. Prog Oceanogr. 1981;10(1):1–70.
6. Satarug S, Garrett SH, Sens MA, Sens DA. Cadmium, environmental exposure, and health outcomes. Environ Health Perspect. 2010;118(2):182–90.
7. Nishijo M, Nakagawa H. Effects of cadmium exposure on life prognosis. Cadmium Toxicity. Singapore: Springer; 2019. p. 63–73.
8. Waalkes MP. Cadmium carcinogenesis in review. J Inorg Biochem. 2000;79(1–4):241–4.
9. Wang C, Sheng J, Hong Y, Peng K, Wang J, Wu D, et al. Molecular characterization and expression of metallothionein from freshwater pearl mussel, Hyriopsis schlegelii. Biosci Biotechnol Biochem. 2016;80(7):1327–35.
10. Couillard Y, Campbell PGC, Tessier A. Response of metallothionein concentrations in a freshwater bivalve (Anodonta grandis) along an environmental cadmium gradient. Limnol Oceanogr. 1993;38(2):299–313.
11. JECFA, Joint FAO/WHO. Food Standards Programme Codex Alimentarius Commission, Report of the 38th session of the Codex Committee on Food Additives and Contaminants, LINORM 06/12A. 2006.
12. FSSAI, Food Safety, and Standards (Contaminants, Toxins, and Residues) Regulations 2011, Notification No. 2-15015/30/2010.
13. Li L, Hu B, Xia L, Jiang Z. Determination of trace Cd and Pb in environmental and biological samples by ETV-ICP-MS after single-drop microextraction. Talanta. 2006;70(2):468–73.
14. Soylak M, Kars A, Narin I. Coprecipitation of Ni^{2+}, Cd^{2+} and Pb^{2+} for preconcentration in environmental samples prior to flame atomic absorption spectrometric determinations. J Hazard Mater. 2008;159(2):435–9.
15. Suleiman JS, Hu B, Huang C, Zhang N. Determination of Cd, Co, Ni and Pb in biological samples by microcolumn packed with black stone (Pierre noire) online coupled with ICP-OES. J Hazard Mater. 2008;157(2):410–7.
16. Chen W, Fang X, Li H, Cao H, Kong J. A simple paper-based colorimetric device for rapid mercury (II) assay. Sci Rep. 2016;6(1):31948.
17. Cate DM, Dungchai W, Cunningham JC, Volckens J, Henry CS. Simple, distance-based measurement for paper analytical devices. Lab Chip. 2013;13(12):2397–404.
18. Yan J, Ge L, Song X, Yan M, Ge S, Yu J. Paper-based electrochemiluminescent 3D immunodevice for lab-on-paper, specific, and sensitive point-of-care testing. Chem Eur J. 2012;18(16):4938–45.
19. He M, Liu Z. Based microfluidic device with upconversion fluorescence assay. Anal Chem. 2013;85(24):11691–4.
20. Ge L, Yan J, Song X, Yan M, Ge S, Yu J. Three-dimensional paper-based electrochemiluminescence immunodevice for multiplexed measurement of biomarkers and point-of-care testing. Biomaterials. 2012;33(4):1024–31.
21. Cheng CM, Martinez AW, Gong J, Mace CR, Phillips ST, Carrilho E, et al. Paper-based ELISA. Angew Chem Int Ed. 2010;49(28):4771–4.
22. Lopez-Ruiz N, Curto VF, Erenas MM, Benito-Lopez F, Diamond D, Palma AJ, et al. Smartphone-based simultaneous pH and nitrite colorimetric determination for paper microfluidic devices. Anal Chem. 2014;86(19):9554–62.
23. Sener G, Uzun L, Denizli A. Colorimetric sensor array based on gold nanoparticles and amino acids for identification of toxic metal ions in water. ACS Appl Mater Interfaces. 2014;6(21):18395–400.
24. Homaei A. Immobilization of Penaeus merguiensis alkaline phosphatase on gold nanorods for heavy metal detection. Ecotoxicol Environ Saf. 2017;136:1–7.
25. Lei C, Dai H, Fu Y, Ying Y, Li Y. Colorimetric sensor array for thiols discrimination based on urease–metal ion pairs. Anal Chem. 2016;88(17):8542–7.
26. Tang Z, Chen H, He H, Ma C. Assays for alkaline phosphatase activity: progress and prospects. Trends Anal Chem. 2019;113:32–43.

27. Aldewachi H, Chalati T, Woodroofe M, Bricklebank N, Sharrack B, Gardiner P. Gold nanoparticle-based colorimetric biosensors. Nanoscale. 2018;10(1):18–33.
28. Shi X, Gu W, Li B, Chen N, Zhao K, Xian Y. Enzymatic biosensors based on the use of metal oxide nanoparticles. Microchim Acta. 2014;181(1–2):1–22.
29. Rahman MM, Ahmed J, Asiri AM. Development of creatine sensor based on antimony-doped tin oxide (ATO) nanoparticles. Sensors Actuators B Chem. 2017;242:167–75.
30. Wang Z, Wang K, Zhao L, Chai S, Zhang J, Zhang X, et al. A novel sensor made of antimony doped tin oxide-silica composite sol on a glassy carbon electrode modified by single-walled carbon nanotubes for detection of norepinephrine. Mater Sci Eng C. 2017;80:180–6.
31. Li Y, Sun J, Mao W, Tang S, Liu K, Qi T, et al. Antimony-doped tin oxide nanoparticles as peroxidase mimics for paper-based colorimetric detection of glucose using smartphone read-out. Microchim Acta. 2019;186(7):403.
32. Pal S, Bhand S. Zinc oxide nanoparticle-enhanced ultrasensitive chemiluminescence immunoassay for the carcinoma embryonic antigen. Microchim Acta. 2015;182(9–10):1643–51.
33. Krishnakumar T, Jayaprakash R, Pinna N, Phani AR, Passacantando M, Santucci S. Structural, optical and electrical characterization of antimony-substituted tin oxide nanoparticles. J Phys Chem Solids. 2009;70(6):993–9.
34. Müller V, Rasp M, Štefanić G, Ba J, Günther S, Rathousky J, et al. Highly conducting nanosized monodispersed antimony-doped tin oxide particles synthesized via nonaqueous sol−gel procedure. Chem Mater. 2009;21(21):5229–36.
35. Kuck JFR, Yu N-T, Askren CC. Total sulfhydryl by Raman spectroscopy in the intact lens of several species: variations in the nucleus and along the optical axis during aging. Exp Eye Res. 1982;34(1):23–37.
36. Swain KK, Balasubramaniam R, Bhand S. A portable microfluidic device-based Fe_3O_4–urease nanoprobe-enhanced colorimetric sensor for the detection of heavy metals in fish tissue. Prep Biochem Biotechnol. 2020;50:1000–13.
37. Treviño S, Andrade-García A, Herrera Camacho I, León-Chavez BA, Aguilar-Alonso P, Flores G, et al. Chronic cadmium exposure lead to inhibition of serum and hepatic alkaline phosphatase activity in Wistar rats. J Biochem Mol Toxicol. 2015;29(12):587–94.
38. Du J, Hu X, Zhang G, Wu X, Gong D. Colorimetric detection of cadmium in water using L-cysteine functionalized gold–silver nanoparticles. Anal Lett. 2018;51(18):2906–19.
39. Song S, Zou S, Zhu J, Liu L, Kuang H. Immunochromatographic paper sensor for ultrasensitive colorimetric detection of cadmium. Food Agric Immunol. 2018;29(1):3–13.
40. Luan Y, Lu A, Chen J, Fu H, Xu L. A label-free aptamer-based fluorescent assay for cadmium detection. Appl Sci. 2016;6(12):432.
41. Gan Y, Liang T, Hu Q, Zhong L, Wang X, Wan H, et al. In-situ detection of cadmium with aptamer functionalized gold nanoparticles based on smartphone-based colorimetric system. Talanta. 2020;208:1202–31.
42. Silwana B, Van Der Horst C, Iwuoha E, Somerset V. Amperometric determination of cadmium, lead, and mercury metal ions using a novel polymer immobilised horseradish peroxidase biosensor system. J Environ Sci Health A. 2014;49(13):1501–11.
43. Meredith NA, Volckens J, Henry CS. Based microfluidics for experimental design: screening masking agents for simultaneous determination of Mn (II) and Co (II). Anal Lett. 2017;9(3):534–40.
44. Xiao N, Dong JX, Liu SG, Li N, Fan YZ, Ju YJ, et al. Multifunctional fluorescent sensors for independent detection of multiple metal ions based on Ag nanoclusters. Sensors Actuators B Chem. 2018;264:184–92.

Publisher's note Springer Nature remains neutral with regard to jurisdictional claims in published maps and institutional affiliations.